

## ORBITAL VARIABILITY IN THE WIND OF THE MASSIVE X-RAY BINARY HD 153919/4U 1700–37<sup>1</sup>

G. HAMMERSCHLAG-HENSBERGE

Astronomical Institute, University of Amsterdam

IAN D. HOWARTH<sup>2</sup>

Joint Institute for Laboratory Astrophysics, University of Colorado, and National Institute of Standards and Technology

AND

TIMOTHY R. KALLMAN

LHEA, NASA/Goddard Space Flight Center

Received 1989 February 16; accepted 1989 September 9

### ABSTRACT

Forty high-dispersion *IUE* spectra of HD 153919, the Of-type primary in the 4U 1700–37 X-ray binary system, have been examined for evidence of orbital profile variability associated with the Hatchett-McCray effect. Although the effect is negligible in the resonance lines of C IV, Si IV, and N V, some subordinate lines show clear orbital changes. The variability in the absorption profile of N IV  $\lambda$ 1718, in particular, is shown to be in agreement with model calculations. The interstellar spectrum is studied, and highly ionized species are shown to be capable of being maintained by the primary's radiation field alone.

*Subject headings:* stars: individual (HD 153919) — stars: winds — ultraviolet: spectra — X-rays: binaries

### I. INTRODUCTION

The 3.4 day X-ray eclipsing binary system 4U 1700–37 was discovered by Jones *et al.* (1973). Since the optical counterpart, HD 153919, is a bright early-type star ( $m_V = 6.6$ ; spectral type O6.5 Ia f<sup>+</sup>, Walborn 1973), high-dispersion *IUE* observations are possible; first results were reported by Dupree *et al.* (1978). The system has also been intensively studied in the optical (e.g., Hammerschlag-Hensberge 1978; van Paradijs, Hammerschlag-Hensberge, and Zuiderwijk 1978) and X-ray (e.g., White, Kallman, and Swank 1983; Gottwald, White, and Stella 1986) spectral regions.

Strong orbital variations are found in the UV resonance lines of C IV, N V, and Si IV of massive X-ray binaries: HD 77581 (Vela X-1/4U 0900–40; Dupree *et al.* 1980); Sk 160 (SMC X-1; Hammerschlag-Hensberge, Kallman, and Howarth 1984); HDE 226868 (Cyg X-1; Davis and Hartmann 1983); and LMC X-4 (Bonnet-Bidaud *et al.* 1981; for reviews see Hammerschlag-Hensberge 1980, or Córdova and Howarth 1987). These variations can be understood in terms of the Hatchett-McCray effect (Hatchett and McCray 1977): a collapsar X-ray source embedded in a stellar wind has a significant effect on the ionization balance in that wind, resulting in observable orbital variations of the UV P Cygni profiles (see, e.g., Dupree *et al.* 1980 for a more detailed description). However, no discernible variations of the Si IV and C IV resonance lines were found for HD 153919 by Dupree *et al.* (1978, 1980). This result can be understood in terms of the very strong, dense stellar wind of the star which gives rise to heavy saturation in these lines. The additional ionization produced by the rather weak X-ray source ( $L_X \sim 10^{36}$  ergs<sup>-1</sup>) must remove some fraction of the parent ions, but the residual optical depth is great enough that the lines remain saturated, and phase-dependent variability is not seen. The strong stellar

wind and low X-ray luminosity suggest the X-ray source is driven by the capture of wind material, rather than through classical lobe overflow (Pettersen 1978; Conti 1978).

We undertook a reexamination of our old *IUE* spectra HD 153919 when improved reduction techniques became available; in addition to 30 high-dispersion spectra taken in 1978–1979, a selection of new spectra obtained in 1985 has also been analyzed. (These recent data were obtained by us at the same time as the long *EXOSAT* observation discussed by Haberl, White, and Kallman 1989; a detailed comparison of the UV and X-ray results will be the subject of a later paper.) The results confirm the near-constancy of C IV and Si IV reported by Dupree *et al.* (1978) but reveal clear variations in some subordinate lines (see Howarth, Hammerschlag-Hensberge, and Kallman 1986). In § II we describe the reduction techniques used for the high-dispersion spectra, and we discuss these data in § III and § IV. Results from low-dispersion spectra are given in § V, and § VI contains an analysis of the interstellar spectrum.

### II. DATA REDUCTION

Table 1 summarizes the spectra used in this study. We have reanalyzed the early spectra (which we obtained during a multiwavelength international observing campaign in 1978) using improved reduction techniques and have added some spectra from the *IUE* archive.

The high-dispersion spectra were all extracted using J. R. Giddings's IUEDR program (Giddings 1983). Each image was checked by eye for gross errors (e.g., microphonic readout noise), and invalid data were edited out. A cross-dispersion scan was then used to locate a short-wavelength order and thereby register the initial extraction template with the spectrum.

Order-by-order extraction was performed using the IUEDR centroid tracking algorithm to center accurately the "extraction slit" on each order. A sampling rate of  $\sqrt{2}$  pixels was used. All pixels flagged as affected by saturation, fiducial

<sup>1</sup> Based on observations made by the *International Ultraviolet Explorer*, collected at the Villafranca Satellite Tracking Station of the European Space Agency and at the Goddard Space Flight Center.

<sup>2</sup> 1988–1989 JILA Visiting Fellow.

TABLE 1  
*IUE* OBSERVATIONS OF HD 153919

Image Number <sup>a</sup>	JD (Start exposure) 2,440,000 +	Exposure (s)	Dispersion <sup>b</sup>	Orbital Phase <sup>c</sup>	Remarks <sup>d</sup>
1476s.....	3632.60	2400	H	0.80	
1513s.....	3638.40	2100	H	0.50	DB
1714s.....	3664.03	2040	H	0.02	DB
1960l.....	3700.26	1200	H	0.63	Xc
1961l.....	3700.30	1080	H	0.65	Xc
1969l.....	3701.02	1320	H	0.86	Xc
1970l.....	3701.08	1080	H	0.87	Xc
1971l.....	3701.18	13	L	0.90	Xc
1972s.....	3701.22	1620	H	0.92	Xc
1973s.....	3701.27	1620	H	0.93	Xc
1974l.....	3701.32	20	L	0.94	Xc
1975s.....	3701.39	3600	H	0.97	Xc
1981l.....	3702.18	18	L	0.20	Xc
1982s.....	3702.22	1620	H	0.21	Xc
1983s.....	3702.26	1620	H	0.22	Xc
1984l.....	3702.31	18	L	0.23	Xc
1985l.....	3702.35	30	L	0.24	2 × , Xc
1986s.....	3702.39	2880	H	0.26	Xc
1987s.....	3702.46	2100	H	0.28	Xc
1991s.....	3703.09	1980	H	0.46	Xc
1992s.....	3703.14	1620	H	0.48	Xc
1994s.....	3703.25	1980	H	0.51	Xc
1995s.....	3703.30	1980	H	0.52	Xc
1996l.....	3703.38	32	L	0.55	2 ×
1997l.....	3703.41	32	L	0.56	2 ×
1998l.....	3703.45	32	L	0.57	2 ×
1999l.....	3703.49	32	L	0.58	2 ×
2000l.....	3703.53	32	L	0.59	2 ×
2001l.....	3703.57	16	L	0.60	
2002s.....	3703.60	2400	H	0.62	
2003s.....	3703.69	3600	H	0.64	
2006s.....	3704.06	2100	H	0.75	
2008s.....	3704.14	1980	H	0.77	
2009s.....	3704.19	1980	H	0.79	
2106s.....	3715.31	1800	H	0.04	DB
2153s.....	3720.15	1800	H	0.46	DB
4742s.....	3957.19	2400	H	0.94	DB
4751s.....	3958.03	2400	H	0.19	DB
4752s.....	3958.07	2400	H	0.20	DB
4753s.....	3958.12	2400	H	0.22	DB
5180s.....	4003.03	2280	H	0.38	DB
25596l.....	6161.67	1200	H	0.08	Xe
25597l.....	6161.70	1200	H	0.08	Xe
25598l.....	6161.75	1200	H	0.10	Xe
25599l.....	6161.80	1200	H	0.11	Xe
25600l.....	6161.83	1200	H	0.12	Xe
25617l.....	6162.96	1260	H	0.46	Xe
25618l.....	6163.00	1260	H	0.47	Xe
25619l.....	6163.04	1260	H	0.48	Xe
25620l.....	6163.14	1260	H	0.51	Xe
25621l.....	6163.18	1260	H	0.52	Xe
1816l.....	3701.15	12	L	0.89	L, Xc

<sup>a</sup> All images were taken with the SWP camera except 1816 (LWR). The *s* and *l* suffixes indicate small and large aperture exposures respectively; the small aperture has ~50% transmission.

<sup>b</sup> H means high dispersion ( $R \approx 10^4$ ); L, low dispersion ( $\Delta\lambda \approx 6 \text{ \AA}$ ).

<sup>c</sup> Phases calculated from  $\phi = (\text{JD} - 2,442,476.680) / 3.41180 - E$ ; Branduardi, Mason, and Sanford 1978.

<sup>d</sup> DB means spectrum obtained from the *IUE* data base (all other spectra are from the authors' observing programs); Xc, Xe mean that contemporaneous of simultaneous X-ray observations were made with the *Copernicus* or *EXOSAT* satellites, respectively; 2 × means two exposures where made in the large aperture; and L means an exposure made with the LWR camera.

marks, ITF truncation, or otherwise identified as faulty were rejected at this stage. A wavelength shift of the form  $m\Delta\lambda = \text{constant}$  (where  $m$  is the echelle order number) was made to bring the C II\*  $\lambda 1335.70$  line to its laboratory wavelength. A subsequent check on the wavelength alignment was made using the Al III  $\lambda 1862.79$  line, which was found to have an instrumental mean wavelength of  $1862.76 \text{ \AA}$ , with a standard deviation of  $0.015 \text{ \AA}$  and an extreme range of  $1862.73\text{--}1862.78 \text{ \AA}$ . This shows that the IUEDR dispersion constants give an internally highly consistent wavelength scale, allowing the individual spectra to be combined with confidence.

A first-order correction to the cross-dispersion order overlap problem was made using the algorithm of Bianchi and Bohlin (1984). This algorithm does not give perfect results, as can be seen from inspection of the C IV and Si IV resonance lines, which go slightly below the nominal zero level in the mean spectra (described later). Nonetheless, it seems safe to assume that the zero level is everywhere good to about 5% of the continuum level, or better.

We also implemented a slightly modified version of Barker's (1984) algorithm for optimizing the echelle ripple correction parameter  $K$ . We adopted  $\alpha = 0.856$  for all images, following Ake (1982). We calculated  $K$  at each order overlap ( $N - 1$  calculations for  $N$  orders) and then smoothed the values with a triangular filter with half-width of five orders, incorporating a  $2\sigma$  rejection threshold. For each order the value of  $K$  finally used is the average of the values at each end. In determining the value of  $K$  at each overlap, we used all the points in each order in the overlap region, with each point being weighted according to the inverse of the calculated ripple correction factor. At the longest wavelengths, where the orders do not overlap, we used the end  $1 \text{ \AA}$  of each order (or 10 points, whichever is greater).

Finally, the data were mapped onto a uniform wavelength grid at  $0.05 \text{ \AA}$  intervals, using a triangular filter. Regions of order overlap were combined by again assigned weights proportional to the inverse ripple correction factors.

The reproducibility given by IUEDR's tracking capability, together with the use of the Bianchi-Bohlin and modified Barker algorithms, ensures that the extracted spectra are mutually consistent and of uniformly high quality (substantially better than the original IUESIPS result), and that the data can be differenced or combined with confidence.

### III. HIGH-DISPERSION RESULTS

We used all the high-dispersion data to construct good quality mean spectra for each 0.2 (or smaller) phase interval. For each interval, typically about six spectra were merged using

$$\bar{f}_\lambda = \left[ \sum_i f_\lambda(i) t(i) H_\lambda(i) \right] / \left[ \sum_i \bar{F}(i) t(i) H_\lambda(i) \right],$$

where  $f_\lambda(i)$  is the extracted flux of spectrum  $i$  (in linearized IUE "Flux Numbers" per second);  $t(i)$  is the exposure time;  $H_\lambda(i) = 1(0)$  for good (bad) data; and  $\bar{F}(i)$  is the mean flux in the range  $1300\text{--}1900 \text{ \AA}$ . This approximately weights the spectra by the integrated net flux and gives a mean spectrum which has an average value of 1.0 in the  $1300\text{--}1900 \text{ \AA}$  region. (No correction for orbital motion was applied;  $K_1 \approx 20 \text{ km s}^{-1}$ , or  $\sim 0.1 \text{ \AA}$ , which is much less than the stellar line widths.)

The grand mean of all spectra shows that saturated P Cygni profiles are present at C III  $\lambda 1175$ , N V  $\lambda 1240$ , Si IV  $\lambda 1400$ , and C IV  $\lambda 1550$ , with corresponding maximum velocities in absorp-

tion of  $\sim 2360, 2620, 2290$ , and  $2590 \text{ km s}^{-1}$ , from which we adopt a maximum edge velocity of  $v_* \approx 2600 \text{ km s}^{-1}$ . The terminal velocity is expected to be  $v_\infty \approx 0.85v_* \approx 2200 \text{ km s}^{-1}$  (Howarth and Prinja 1989). Evidence of mass loss is also present in O IV  $\lambda 1340$ , S V(?)  $\lambda 1500$ , He II  $\lambda 1640$ , N IV  $\lambda 1718$ , and N III  $\lambda 1750$  (but not in the Al III  $\lambda 1860$  resonance lines, nor the O V  $\lambda 1370$  or Fe III multiplet UV34 subordinate lines). This emphasizes the extraordinary strength of HD 153919's stellar wind.

Figures 1–9 show the appearance of these mass-loss features at different binary phase intervals. The most important result apparent from these figures is the convincing evidence for phase-related variability in the N IV  $\lambda 1718$  line (Fig. 10). No other line shows such striking changes, although related effects appear to be present in He II  $\lambda 1640$  (Fig. 7), and possibly also in N III  $\lambda 1750$  and S V  $\lambda 1500$  (Figs. 5 and 9).

The top section of Figure 10 shows the N IV line in the average of six 1978 spectra taken near phase zero (i.e., X-ray

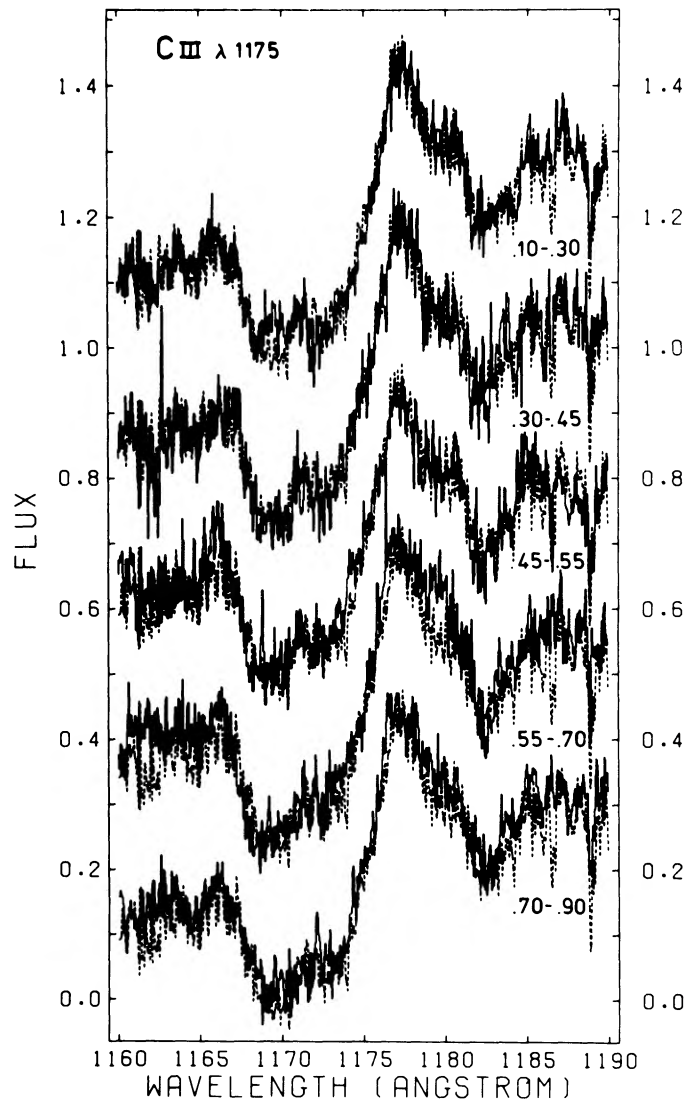


FIG. 1.—Mean spectra of HD 153919 in the region of C III  $\lambda 1175$  for different binary phase intervals. Each mean spectrum is the average of from four to six individual spectra; the dotted spectrum is the mean of six spectra taken during X-ray eclipse ( $\phi 0.9 \rightarrow 0.1$ ).

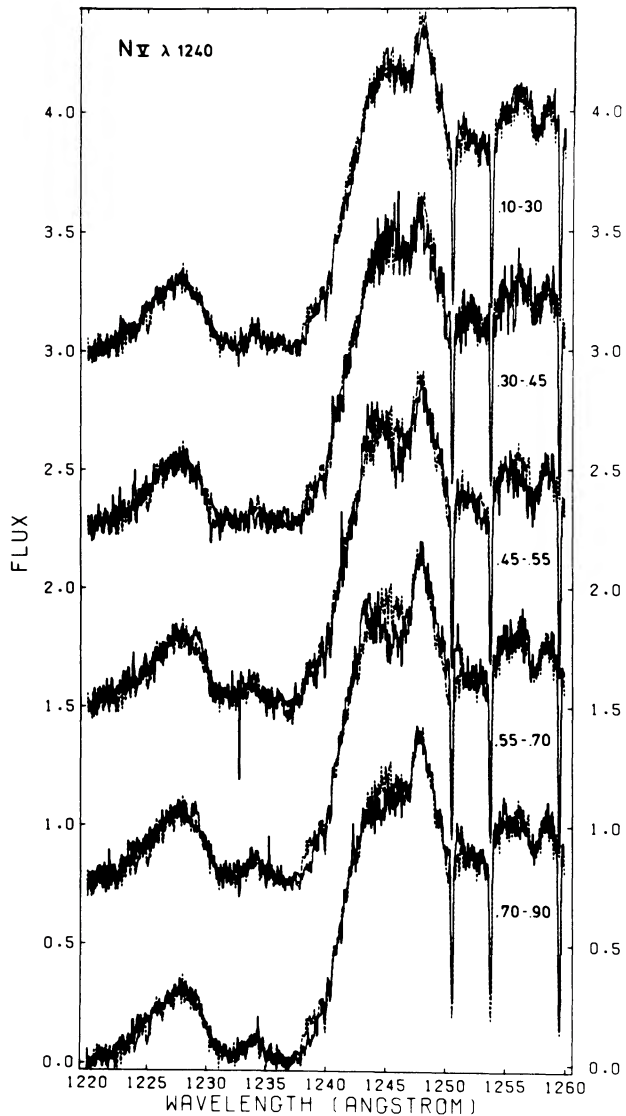


FIG. 2.—Same as Fig. 1, but for N IV  $\lambda 1240$

eclipse, when the “bleaching” effect of the X-ray source is expected to be negligible), and the average of six similar spectra taken near phase 0.5. The bottom section shows corresponding results from spectra taken in 1985. In both cases the absorption component is weaker near phase 0.5, as expected if the origin of the variability is the Hatchett-McCray effect.

To distill the variability into a single number, we fitted a sixth order polynomial to all datum points in the wavelength ranges 1708.5–1709.5 Å and 1710.5–1718.0 Å, then took the value of the fitted function at 1713.25 Å. This quantity is plotted as a function of orbital phase in Figure 11, which confirms the decrease in absorption line strength for phases 0.4 through 0.6. Moreover, Figures 10 and 11 show that the variability repeats at widely separated epochs, confirming that it is attributable to the phase-dependent Hatchett-McCray effect, rather than stochastic changes.

There is evidence that the effect is somewhat stronger in 1978 than in 1985, a result which could be due to a difference in the strength of the X-ray source at the two epochs. G. Branduardi (1988, personal communication) and F. Haberl (1988, personal communication) kindly supplied the X-ray fluxes

recorded by *Copernicus* in 1978 (Branduardi *et al.* 1979) and by *EXOSAT* in 1985 (Haberl, White, and Kallman 1989) close to the times of phase 0.5 ultraviolet observations. The integrated flux observed by *Copernicus* in the energy range 3.1–9.4 keV (not corrected for low-energy absorption) is  $4.1 \times 10^{-9}$  ergs  $\text{cm}^{-2} \text{s}^{-1}$  during JD 2,443,703.14–703.16 ( $\phi = 0.48$ ). During a similar phase interval in 1985, *EXOSAT* (ME experiment) obtained more than 30 spectra; in the same energy range the flux varies over 1.5 orders of magnitude (JD 2,446,162.80–163.24;  $\phi = 0.40 \rightarrow 0.53$ ). Although it is difficult directly to compare results from the two satellites when the X-ray emission is so strongly variable, it seems that the flux observed by *Copernicus* is close to the maximum recorded by *EXOSAT*. The stronger 1978 X-ray flux is therefore in qualitative agreement with the weaker N IV  $\lambda 1718$  absorption profile observed at that time, compared to the 1985 observations.

The He II  $\lambda 1640$  line also shows profile variations which are phase related, but apparently more complex. The undisturbed profile shows two absorption components, one at about 900  $\text{km s}^{-1}$  (the same velocity as the N IV component) which disap-

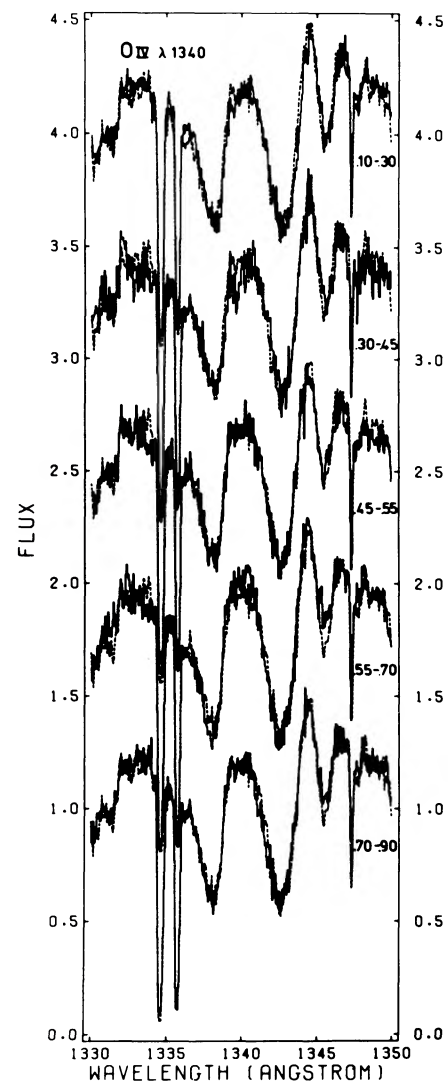


FIG. 3.—Same as Fig. 1, but for O IV  $\lambda 1340$

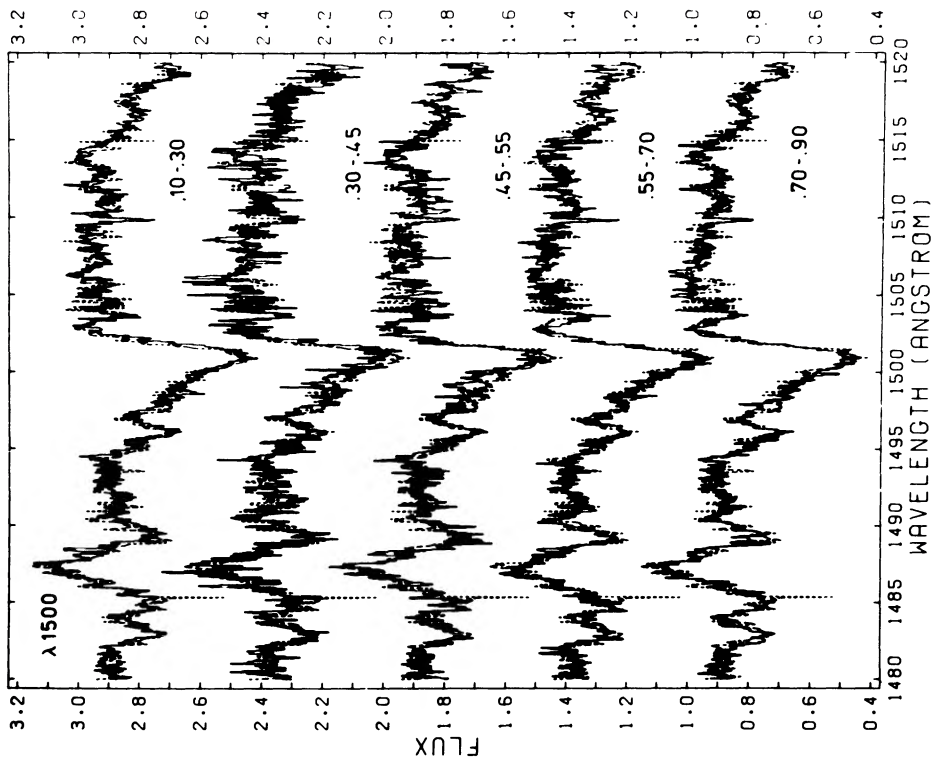


FIG. 5.—Same as Fig. 1, but for Si IV  $\lambda 1500$

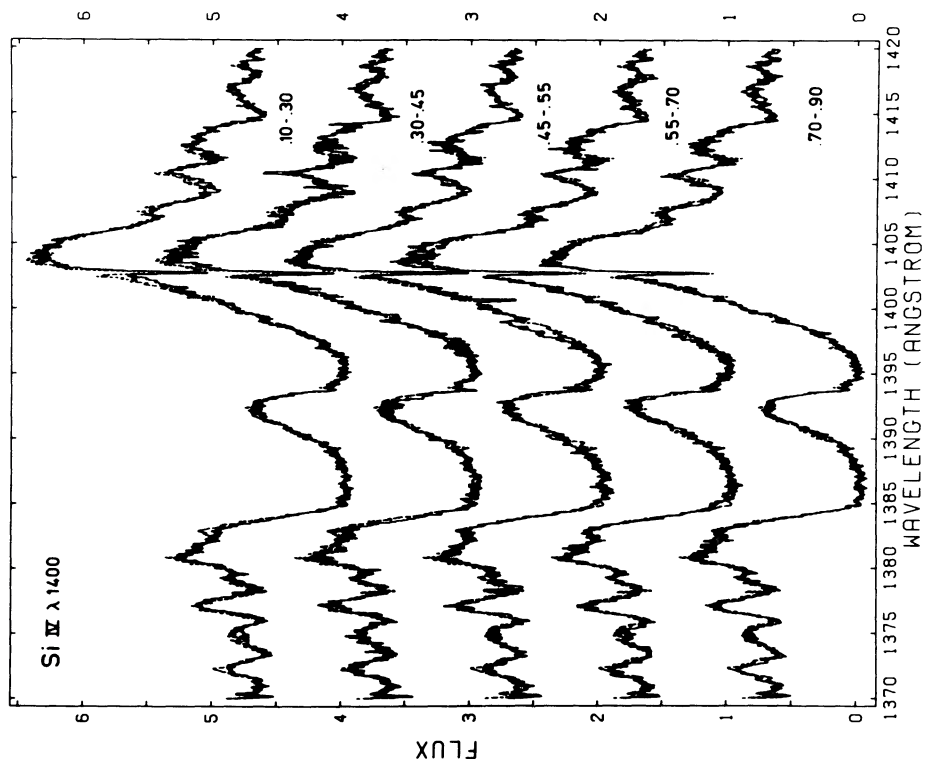


FIG. 4.—Same as Fig. 1, but for Si IV  $\lambda 1400$

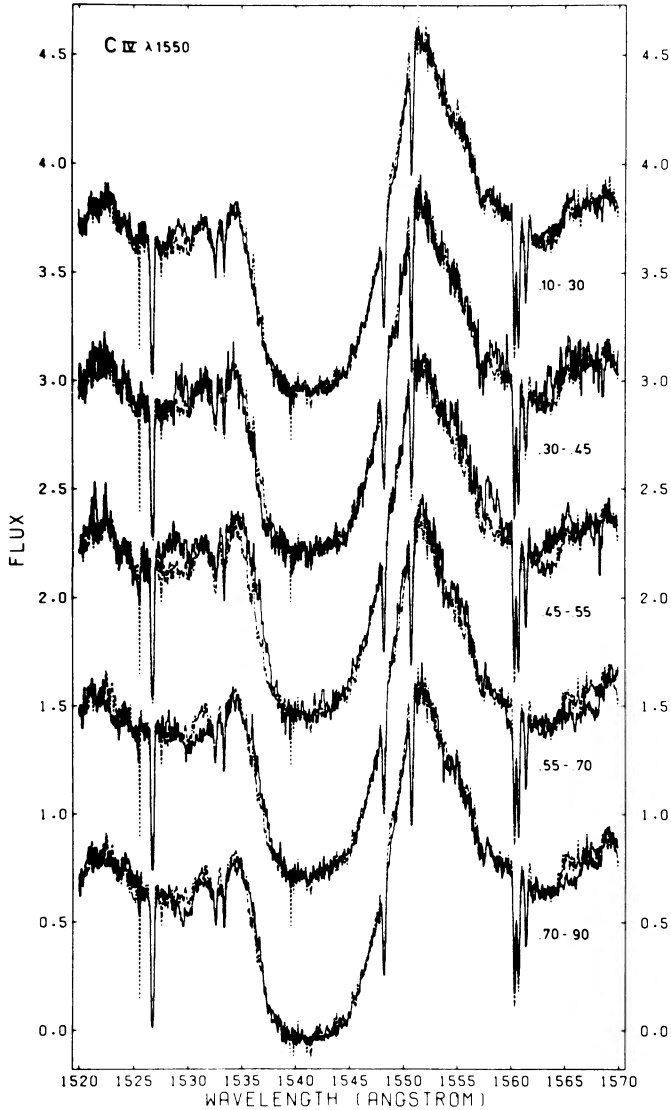


FIG. 6.—Same as Fig. 1, but for C IV  $\lambda 1550$ . Variability in the violet wing of the  $\phi 0.45 \rightarrow 0.55$  spectrum may be due to the Hatchett-McCray effect.

pears at phase 0.5. This is comparable to the N IV behavior and the reverse of the behavior reported for He I  $\lambda 5876$  and H $\alpha$   $\lambda 6560$  by Fahlman and Walker (1980), i.e., and extra absorption component appearing at  $\phi \approx 0.6$ , which they interpreted as evidence for a gas stream from the inner Lagrangian point. Further details of the wind structure come from a detailed analysis of *EXOSAT* observations of a complete orbital cycle (Haberl, White, and Kallman 1989).

#### IV. MODELING THE N IV LINE

The variability in N IV is similar to that seen in the resonance lines of C IV and Si IV in other massive X-ray binaries (Hammerschlag-Hensberge 1980), and is qualitatively consistent with the “bleaching” of  $N^{3+}$  ions in a zone in the wind surrounding the X-ray source (Hatchett and McCray 1977). We have therefore calculated the N IV profile variability expected on the basis of this model to see if the results are indeed consistent with the observed effects.

Our modeling procedure is as follows. (1) We assume that the observed N IV profile at phase zero reflects the distribution

of  $N^{3+}$  ions with velocity in the absence of X-ray ionization and fit the models of Olson (1981) to this profile. This yields a value for the parameter  $T$ , which is proportional to the radial optical depth in the line. (2) We then construct models for the phase 0.5 profile by assuming that at each point in the wind the abundance of  $N^{3+}$  ions is given by either the undisturbed wind fit (from step [1]) or by X-ray photoionization theory, whichever is smaller. The X-ray ionization is most important inside a roughly spherical “Strömgen zone” which surrounds the X-ray source and which turns out to be comparable to the primary star in size. The size of this region (and therefore the extent of the X-ray-induced line suppression) depends on the ratio of the X-ray source luminosity,  $L_X$ , to the wind density; given the run of velocity with radius, and assuming a spherically symmetric steady-state flow, this is equivalent to the ratio of  $L_X$  to the mass-loss rate,  $\dot{M}$ . We adopt a velocity law of the canonical form

$$v(r) = v_*(1 - R_*/R)^\beta,$$

where  $\beta$  is believed to have values in the range 0.5–1 for the winds of single O stars (e.g., Pauldrach, Puls, and Kudritzki 1986). More details of the photoionization model and line

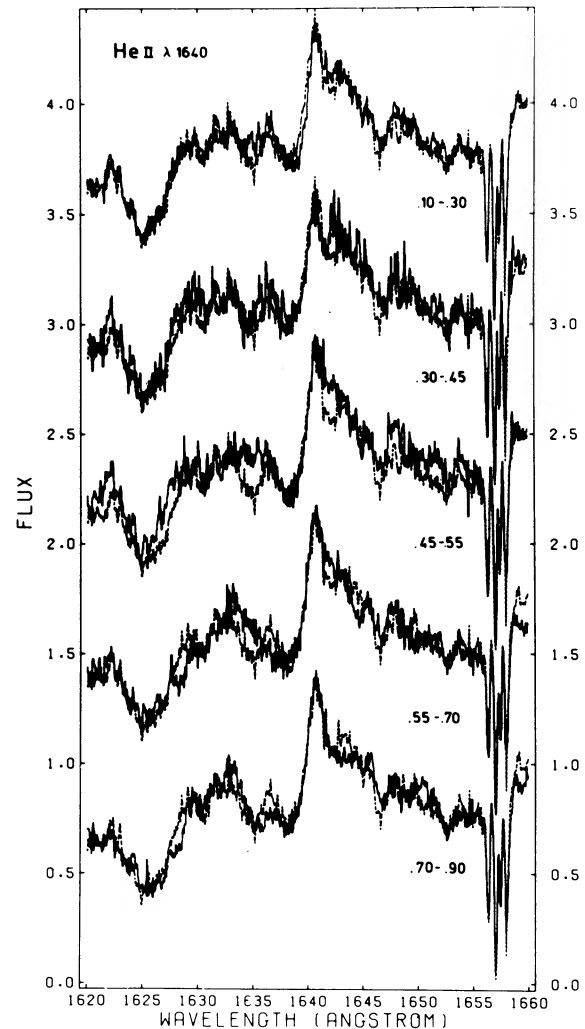


FIG. 7.—Same as Fig. 1, but for He II  $\lambda 1640$ . Phase-dependent variability is present.

profile modeling procedure are described in Kallman and McCray (1982) and McCray *et al.* (1984).

Results are illustrated in Figure 12. The upper section shows the results of modeling the phase zero profile. An acceptable fit is found using Olson's models with an optical depth parameter  $T = 5$ ; the fit is significantly improved if we assume a "core" N IV absorption line. (This assumption is supported by the observation of a strong N IV photospheric line in the spectra of main-sequence stars of similar  $T_{\text{eff}}$ .) At low velocities (both positive and negative), the observed profile is not very well matched, but this failure is typical of models calculated using the Sobolev approximation and monotonic velocity laws, and is not specific to the present case. We were also unable to match the absorption profile at velocities more negative than about  $-2000 \text{ km s}^{-1}$  ( $\sim 0.7v_*$ ); here the observed profile shows an absorption dip, while the model profiles all how a monotonic increase in residual intensity with  $|v|$ . Almost certainly there is a blend with a photospheric line at  $\sim 1707 \text{ \AA}$ , since it is difficult to understand what excitation mechanisms could produce N IV absorption at such high velocities.

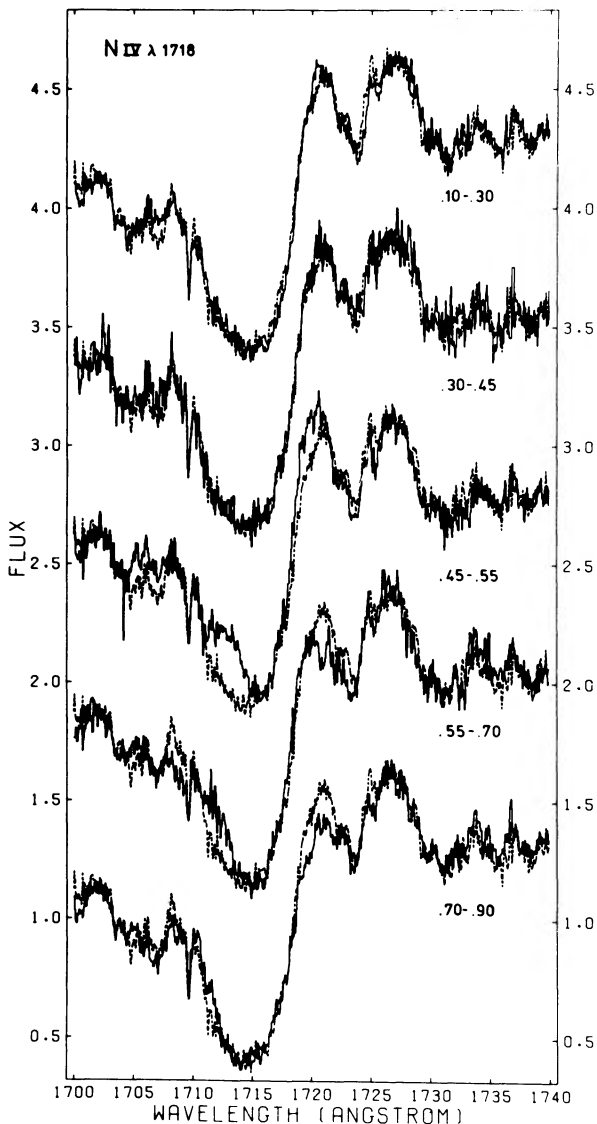


FIG. 8.—Same as Fig. 1, but for N IV  $\lambda 1718$ . A weakening of the absorption profile due to the Hatchett-McCray effect is clearly visible around phase 0.5.

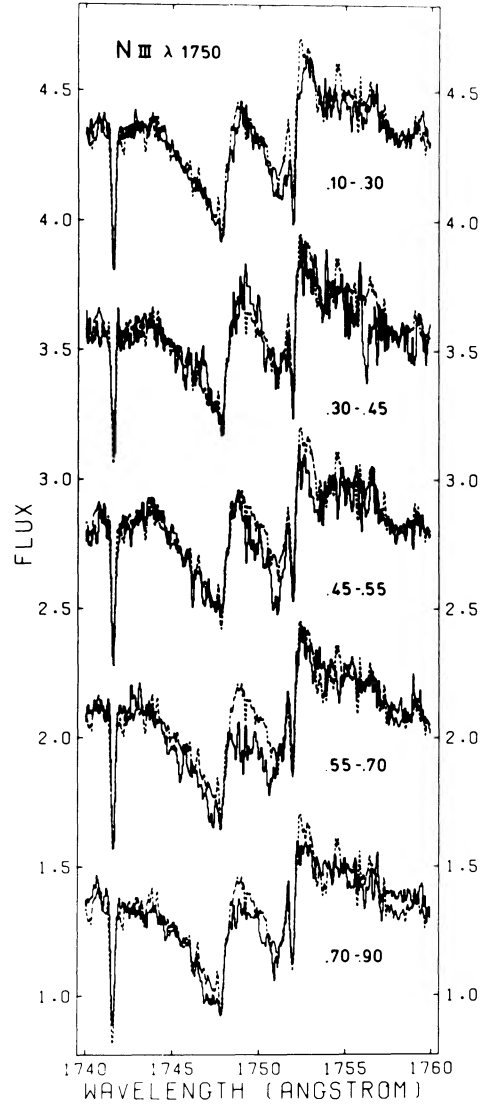


FIG. 9.—Same as Fig. 1, but for N III  $\lambda 1750$

The lower part of Figure 12 shows our best fit to the observed profile at phase 0.5. The systematic discrepancies noted for the phase zero profile are still present, but the *variation* in the observed profile is rather well matched by the change in the theoretical profiles. In particular, the increase in residual intensity around  $-1000 \text{ km s}^{-1}$  is reproduced in some detail. The wavelength dependence of the profile variability yields the wind velocity at the X-ray source and thereby constrains the index  $\beta$ . Since a comparison of the phase zero and phase 0.5 profiles shows that the X-ray-induced suppression of the absorption, and hence the X-ray ionization, occurs at  $\sim 0.4 v_*$ , the orbital separation (adopted from Conti 1978) *requires*  $\beta \approx 1$ . An attempt to fit the profile with a  $\beta = 0.5$  law, for example, would yield X-ray induced suppression at  $\sim 0.7v_*$ , a much greater velocity than is observed.

It is interesting to note that the value of  $\beta$  which we obtain is consistent with dynamical models for the winds of single OB stars (e.g., Pauldrach, Puls, and Kudritzki 1986), but differs from that inferred from X-ray observations of 4U 1700-37 ( $\beta \approx 0.5$ ; Haberl, White, and Kallman, 1989). We suspect that this difference is due to the fact that X-ray studies can sample

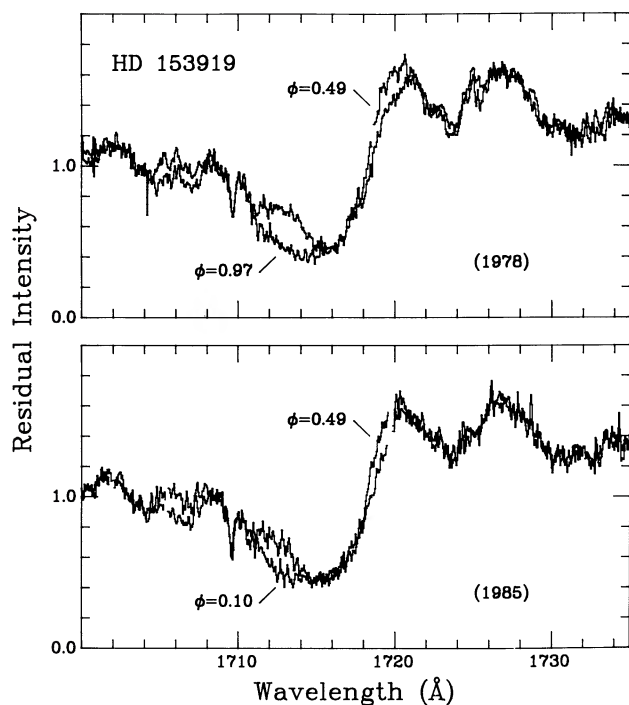


FIG. 10.—Orbital variability in the N IV  $\lambda 1718$  line, due to the Hachett-McCray effect. Each spectrum is the mean of six individual spectra in the given phase interval. *Top*: spectra from the 1978 campaign; *bottom*: spectra from the 1985 observing campaign. The amplitude of the variability is slightly different in the two data sets.

the wind very close to the X-ray source, where the dynamics will differ from those of a single O star, while the UV line profile is formed over a large fraction of the wind volume, where our assumption of spherical symmetry is more nearly correct.

Our best-fit model requires a ratio of the mass-loss rate to the X-ray luminosity of  $\dot{M}/L_X \approx 5 \times 10^{41} (M_\odot \text{ yr}^{-1})/(\text{ergs s}^{-1})$ . While the fit does not reproduce the *detailed* shape of the observed absorption profile, as noted previously, it is accept-

able at the level at which we are able to model X-ray-photoionized winds, showing that the adopted parameters are all generally consistent with results of the N IV observations. In particular, the required ratio of  $\dot{M}/L_X$  is in agreement with the observed X-ray flux of  $\sim 10^{-9} \text{ ergs cm}^{-2} \text{ s}^{-1}$ , the distance (§ V), and the mass-loss rate ( $\dot{M} \approx 6 \times 10^{-6} M_\odot \text{ yr}^{-1}$ ; Howarth and Prinja 1989). The differences in detail between the observed and modeled profiles could be due to a variety of factors neglected in the models: density inhomogeneities due to shocks, or other departures from the simple velocity law adopted; the affects of wind dynamics of the gravitational field of the secondary or of the X-ray photoionization it produces; beamed X-rays; etc. Modeling these factors is beyond the scope of the present paper.

#### V. LOW-DISPERSION SPECTRA

Shortly before our 1978 July observations were made, Matilsky and Jessen (1978) claimed the discovery of a 97 minute periodicity in the X-ray flux from 4U 1700-37 (see also Matilsky, La Sala, and Jessen 1978); Kruszewski (1978) reported a similar period in optical data, with the largest amplitude occurring at phase 0.5. This prompted the procurement of a large number of low-resolution spectra around phase 0.5 during our 10 day campaign of coordinated observations. Unfortunately, the X-ray periodicity was subsequently shown to be spurious by Hammerschlag-Hensberge, Henrichs, and Shaham (1979), and new optical observations discussed by them, and by van Paradijs and van der Woerd (1982), failed to show any related periodicity.

The low-resolution ( $\Delta\lambda \approx 6 \text{ \AA}$ ) data cover the wavelength range 1150-3200  $\text{\AA}$ . The bulk of the exposures were taken with the short-wavelength prime (SWP) camera ( $\lambda < 1950 \text{ \AA}$ ), with a single spectrum taken with the long-wavelength redundant (LWR) camera (Table 1). All spectra were taken with the large ( $10'' \times 20''$ ) entrance aperture to ensure accurate spectrophotometry; the time-dependent degradation in camera sensitivities does not significantly affect these data. In some cases, two exposures separated by  $\sim 9''$  were made in the large aperture to improve time resolution by reducing overheads in

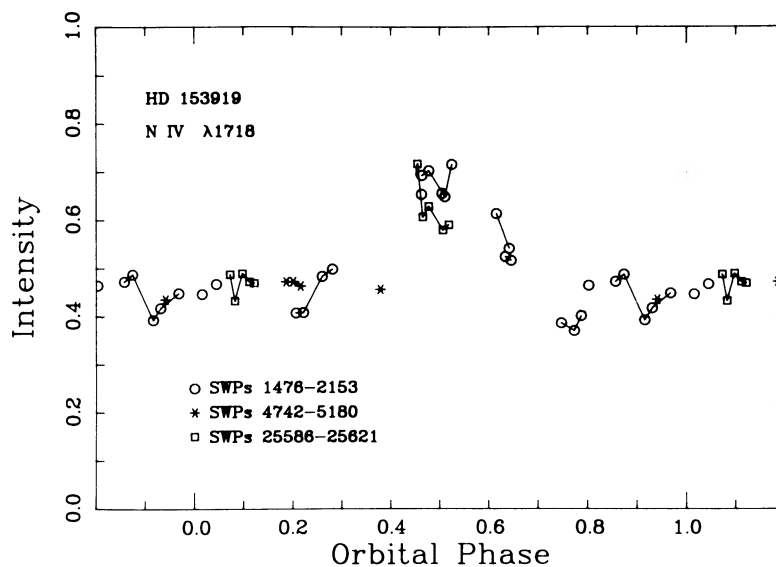


FIG. 11.—The intensity of the N IV  $\lambda 1718$  line at  $1713.25 \text{ \AA}$  as a function of orbital phase (see text for details). Consecutive images are joined by lines. There is a systematic decrease in the absorption line strength for phases  $0.4 \rightarrow 0.6$ ; additional stochastic variability may be present.

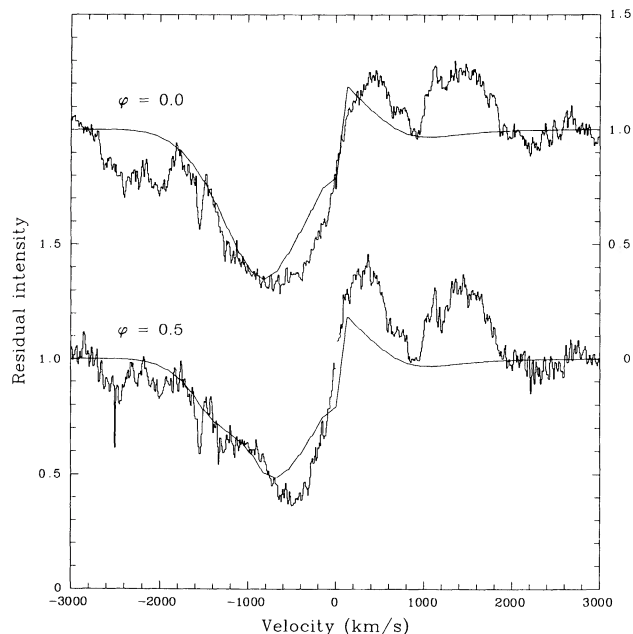


FIG. 12.—Observed and modeled N IV  $\lambda 1718$  profiles. The upper curves (right-hand ordinate) show results at phase zero, when the observed profile is practically undisturbed by the X-ray source. Lower curves (left-hand ordinate) show results for phase 0.5; the reduction in absorption at  $\sim 0.4v_* \approx -1000$  km s $^{-1}$  is well matched by the theoretical calculation.

reading out the cameras; we combined the results of such exposures into a single spectrum. Preliminary extraction of the spectra was carried out at the ESA and NASA ground stations; we corrected all SWP images processed with the incorrect Intensity Transfer Function by using the algorithm described by Cassatella *et al.* (1980) and flux-calibrated the spectra using the calibration of Bohlin *et al.* (1980).

Analysis of these data confirmed the absence of any significant 97 minute periodicity. However, the spectra are still of use in order to investigate the interstellar reddening. To do this we used images SWP 1971 and LWR 1816 (taken at the same binary phase). The low-dispersion spectrum is unremarkable, and shows a strong 2200 Å extinction feature. Rather than attempt a direct comparison of the observed spectrum with model atmosphere fluxes in order to determine the reddening, we took advantage of the fact that the flux distributions of hot stars are essentially linear in a  $\log f_\lambda$  versus  $\lambda$  plot in the wavelength range  $\sim 1900$ – $3000$  Å. [For example, a Kurucz 1979 35,000 K,  $\log(g) = 3.5$  model gives a linear correlation coefficient of  $r = 0.9995$ .] We binned the data into 50 Å bands, omitting those with strong spectral features, then fitted straight lines to the binned data for various amounts of dereddening, using Seaton's (1979) formula. The largest correlation coefficient corresponds to our best estimate of  $E_{B-V} : 0.53 \pm 0.03$ . This value is in excellent agreement with the estimate of  $E_{B-V} = 0.52$  estimated by Hammerschlag-Hensberge and Wu (1976) from *ANS* ultraviolet photometry. Using the relationship between distance and  $A_V$  given by Neckel and Klare (1980) for this region of sky results in a distance estimate of  $0.8 \pm 0.2$  kpc, roughly half previously suggested values based on reddening values obtained from optical data.

## VI. THE INTERSTELLAR SPECTRUM

As expected for a star with moderately heavy reddening, HD 153919 displays a rich interstellar spectrum of lines of H I

TABLE 2  
EQUIVALENT WIDTHS FOR SELECTED  
INTERSTELLAR LINES

Spectrum	Line	$W_\lambda$ (mÅ)
C I .....	1194.0	$63 \pm 9$
	1276.5	$53 \pm 10$
	1280.1	$54 \pm 5$
	1328.8	$154 \pm 15$
	1560.3	$191 \pm 20$
C IV .....	1548.2	$194 \pm 9$
	1550.8	$107 \pm 4$
N V .....	1242.8	$< 20$
Mg I .....	2852.1	$524 \pm 52$
Mg II .....	1239.9	$84 \pm 13$
	1240.4	$65 \pm 13$
	2795.5	$729 \pm 74$
	2802.7	$745 \pm 77$
Al III .....	1854.7	$280 \pm 20$
	1862.8	$200 \pm 10$
Si II .....	1304.4	$243 \pm 5$
	1526.7	$328 \pm 11$
	1808.0	$281 \pm 5$
Si II* .....	1194.5	$107 \pm 11$
	1264.7	$64 \pm 4$
Si III .....	1206.5	$255 \pm 18$
Si IV .....	1393.8	$141 \pm 34$
	1402.8	$103 \pm 11$
Fe II .....	1608.5	$279 \pm 10$
	2343.5	$471 \pm 46$
	2373.7	$374 \pm 30$
	2382.0	$545 \pm 37$
	2585.9	$462 \pm 13$
	2599.4	$562 \pm 22$

NOTE.—Quoted errors are 90% confidence intervals, after Howarth and Phillips 1986. The N V upper limit is a  $3\sigma$  value.

species. In addition, the CO fourth positive series is present, together with relatively strong lines due to high ions ( $IP > 13.6$  eV). Table 2 lists equivalent widths for selected lines, measured from the grand average spectrum formed from all data. The neutral hydrogen column, estimated from Ly $\alpha$   $\lambda 1216$  by dividing the observed profile by theoretical fully damped profiles until a "flat" continuum is restored, is  $N(\text{H}^0) = 21.4 \pm 0.1$  dex cm $^{-2}$ .

No unblended lines show evidence for velocity structure or asymmetries at the resolution afforded by *IUE*. We have therefore analyzed the interstellar spectrum assuming a simple single-cloud model with a Maxwellian velocity distribution for the absorbers (see Howarth and Phillips 1986 for details; all atomic data were taken from this source). A single-cloud model will provide lower limits to true column densities if (as is certainly true) the sightline is in reality more complex (Nachmann and Hobbs 1973); however, for reasonable distributions of bulk cloud velocities and internal velocity structure, the single-cloud model is unlikely to give grossly erroneous results (Jenkins 1986).

The Mg II lines are particularly useful for constraining model parameters. The  $\lambda 1240$  lines are relatively weak, and their equivalent widths are primarily sensitive to column density,  $N$ , while the  $\lambda 2800$  lines are saturated; their equivalent widths are sensitive to the velocity dispersion parameter,  $b$ , but

TABLE 3  
MODEL PARAMETERS FOR  
INTERSTELLAR SPECIES

Ion	$b$ ( $\text{km s}^{-1}$ )	$N$ ( $\text{dex cm}^{-2}$ )
C <sup>+</sup> .....	>8 (10)	14.7-14.4 (14.7±0.1)
Mg <sup>0</sup> .....	(10)	(14.9±0.3)
Mg <sup>+</sup> .....	10±1	16.7±0.1
Si <sup>+</sup> .....	10-15 (10)	16.9-15.7 (16.9±0.3)
Fe <sup>+</sup> .....	9-17 (10)	16.6-14.6 (16.3±0.3)
C <sup>3+</sup> .....	20-150 (22)	13.9-13.7 (13.8±0.1)
N <sup>4+</sup> .....	...	<13.3
Al <sup>2+</sup> .....	(22)	(13.5±0.1)
Si <sup>++</sup> .....	<10 (5)	>12.9 (13.4±0.3)
Si <sup>2+</sup> .....	>20 (30)	13.6-13.1 (13.4±0.1)
Si <sup>3+</sup> .....	2-100 (22)	15.9-13.3 (13.45±0.1)
S <sup>2+</sup> .....	20:	≤15.6:

NOTE.—Ranges of  $b$  and  $N$  quoted are those which reproduce the observed equivalent widths acceptably well. Parenthesized values use  $b$  constrained from profile fits and/or from the requirement that H I region species have the same  $b$  value.

are insensitive to  $N$ . A single-cloud model which matches the equivalent widths of all four lines within the quoted errors requires  $b = 10 \pm 1 \text{ km s}^{-1}$  (and  $N = 16.7 \pm 0.1 \text{ dex cm}^{-2}$ ). Curve-of-growth analyses of other H I region species are consistent with this value (Table 2). Model line profiles require  $b \simeq 10 \text{ km s}^{-1}$  for all species [using  $b(\text{inst}) = 18 \text{ km s}^{-1}$ ; Howarth and Phillips 1986]. Derived column densities are given in Table 3 (where the quoted errors allow for both the uncertainties on the measured equivalent widths and for a range of  $\pm 1 \text{ km s}^{-1}$  in  $b$ ). Gas phase depletions of H I region species are unexceptional.

Of more interest are the highly ionized species present in the spectrum. Doublet ratios constrain  $b$  only weakly (Table 3), but profile-fitting provides tighter limits, requiring  $b = 22 \pm 3 \text{ km s}^{-1}$  for C IV, Si IV, and Al III. [It is noteworthy that  $b(\text{H}^+)$  is

definitely larger than  $b(\text{H}^0)$ , although presumably the highly ionized species are distributed over a smaller spatial domain.] Not all H II region species share the same  $b$ , however (nor, by inference, the same space distribution): the Si III  $\lambda 1206$  profile requires a larger value ( $\sim 30 \text{ km s}^{-1}$ , although the column density is not sensitive to the precise figure), while Si II\*, an H II region species which shows unusually strong lines in the spectrum of HD 153919, requires  $b \leq 10 \text{ km s}^{-1}$  ( $b = 5 \text{ km s}^{-1}$  gives good fits in this case).

Column densities for H II region species are summarized in Table 3. (We include S<sup>2+</sup>, which shows a strong line at 1190.2 Å, blended with Si II  $\lambda 1190.4$ ; the column density is uncertain largely because of problems with oscillator strengths for the Si II lines.) A substantial ionized hydrogen column (in excess of  $\sim 20 \text{ dex cm}^{-2}$ ) is indicated by these data. The Si<sup>2+</sup>, Si<sup>3+</sup>, and C<sup>3+</sup> columns are in reasonable agreement with those expected on the basis of simple homogeneous models of H II regions (Black *et al.* 1980), suggesting that the highly ionized species can be maintained by stellar radiation alone, and that the X-ray source (which is considerably less luminous than the primary) plays only a minor role.

To check this for other species we modified the ionization balance code described by Howarth (1984) to calculate nebular models. The principal modifications were to the density structure (constant density assumed), the stellar radiation field (Kurucz models used rather than black body fluxes), and the diffuse radiation field (which was set to zero). The neglect of the diffuse field in the photoionization integral and the exclusion of charge transfer in the ionization balance means that the results are only approximate, but more elaborate modeling did not seem worthwhile given the uncertainties in the stellar EUV radiation field and the nebular density structure. The calculations confirm that all the observed columns can comfortably be reproduced by a star with  $T_{\text{eff}} \simeq 37,400 \text{ K}$ ,  $R_* \simeq 24 R_{\odot}$  (Howarth and Prinja 1989). The only substantial disagreement between the models and observations is for silicon, where both our models and those of Black *et al.* (1980) predict  $\log N \simeq 15$  for Si<sup>2+</sup> and Si<sup>3+</sup>, some 1.5 dex greater than observed. A likely cause of this discrepancy is depletion of silicon onto grains in the H II region, as in H I regions.

We are grateful to Graziella Branduardi for recovering the *Copernicus* X-ray observations of 4U 1700-37, and Frank Haberl for providing a preprint and details of *EXOSAT* observations. I. D. H. thanks the JILA Fellows for the award of a Visiting Fellowship and T. P. Snow for access to CASA facilities.

#### REFERENCES

- Ake, T. B. 1982, *NASA IUE Newsletter*, No. 19, p. 37.  
 Barker, P. K. 1984, *A.J.*, **89**, 899.  
 Bianchi, L., and Bohlin, R. 1984, *Astr. Ap.*, **134**, 31.  
 Black, J. H., Dupree, A. K., Hartmann, L. W., and Raymond, J. C. 1980, *Ap. J.*, **239**, 502.  
 Bohlin, R. C., Holm, A. V., Savage, B. D., Snijders, M. A. J., and Sparks, W. M. 1980, *Astr. Ap.*, **85**, 1.  
 Bonnet-Bidaud, J. M., Ilovaisky, S. A., Mouchet, M., Hammerschlag-Hensberge, G., van der Klis, M., Glencross, W. M., and Willis, A. J. 1981, *Astr. Ap.*, **101**, 184.  
 Branduardi, G., Dupree, A. K., Sanford, P. W., and Pollard, G. S. G. 1979, *Nature*, **279**, 508.  
 Branduardi, G., Mason, K. O., and Sanford, P. W. 1978, *M.N.R.A.S.*, **185**, 137.  
 Cassatella, A., Holm, A., Ponz, D., and Schiffer, F. H., III. 1980, *ESA IUE Newsletter*, No. 5, p. 5.  
 Conti, P. S. 1978, *Astr. Ap.*, **63**, 225.  
 Córdova, F. A., and Howarth, I. D. 1987, in *The Scientific Accomplishments of IUE*, ed. Y. Kondo (Reidel: Dordrecht), p. 395.  
 Davis, R., and Hartmann, L. 1983, *Ap. J.*, **270**, 671.  
 Dupree, A. K., *et al.* 1978, *Nature*, **275**, 400.  
 Dupree, A. K., *et al.* 1980, *Ap. J.*, **238**, 969.  
 Fahlman, G. G., and Walker, G. A. H. 1980, *Ap. J.*, **240**, 169.  
 Giddings, J. 1983, *ESA IUE Newsletter*, No. 17, p. 53.  
 Gottwald, M., White, N. E., and Stella, L. 1986, *M.N.R.A.S.*, **222**, 21p.  
 Haberl, F., White, N. E., and Kallman, T. R. 1989, *Ap. J.*, **343**, 409.  
 Hammerschlag-Hensberge, G. 1978, *Astr. Ap.*, **64**, 399.  
 ———. 1980, in *Proc. 2nd European IUE Conf.* (ESA SP-157) (Noordwijk: ESA), p. lix.  
 Hammerschlag-Hensberge, G., Henrichs, H. F., and Shaham, J. 1979, *Ap. J. (Letters)*, **228**, L75.  
 Hammerschlag-Hensberge, G., Kallman, T. R., and Howarth, I. D. 1984, *Ap. J.*, **283**, 249.

- Hammerschlag-Hensberge, G., and Wu, C.-C. 1977, *Astr. Ap.*, **56**, 433.  
 Hatchett, S. P., and McCray, R. A. 1977, *Ap. J.*, **211**, 552.  
 Howarth, I. D. 1984, *M.N.R.A.S.*, **211**, 167.  
 Howarth, I. D., Hammerschlag-Hensberge, G., and Kallman, T. 1986, in *New Insights in Astrophysics* (ESA SP-263) (Noordwijk: ESA); p. 475.  
 Howarth, I. D., and Phillips, A. P. 1986, *M.N.R.A.S.*, **222**, 809.  
 Howarth, I. D., and Prinja, R. K. 1989, *Ap. J. Suppl.*, **69**, 527.  
 Jenkins, E. B. 1986, *Ap. J.*, **304**, 739.  
 Jones, C., Forman, W., Tananbaum, H., Schreier, B., Gursky, H., and Kellogg, L. 1973, *Ap. J. (Letters)*, **181**, L43.  
 Kallman, T. R., and McCray, R. 1982, *Ap. J. Suppl.*, **50**, 263.  
 Kruszewski, A. 1978, *Inf. Bull. Var. Stars*, No. 1424.  
 Kurucz, R. 1979, *Ap. J. Suppl.*, **40**, 1.  
 Matilsky, T., La Sala, J., and Jessen, J. 1978, *Ap. J. (Letters)*, **224**, L119.  
 Matilsky, T., and Jessen, J. 1978, *IAU Circ.*, No. 3193.  
 McCray, R., Kallman, T. R., Castor, J. I., and Olson, G. L. 1984, *Ap. J.*, **282**, 245.  
 Nachmann, P., and Hobbs, L. M. 1973, *Ap. J.*, **182**, 481.  
 Neckel, T., and Klare, G. 1980, *Astr. Ap. Suppl.*, **42**, 251.  
 Olson, G. L. 1981, *Ap. J.*, **245**, 1054.  
 Pauldrach, A., Puls, J., and Kudritzki, R. P. 1986, *Astr. Ap.*, **164**, 86.  
 Petterson, J. A. 1978, *Ap. J.*, **224**, 625.  
 Seaton, M. J. 1979, *M.N.R.A.S.*, **187**, 73p.  
 van Paradijs, J., Hammerschlag-Hensberge, G., and Zuiderwijk, E. J. 1978, *Astr. Ap. Suppl.*, **31**, 189.  
 van Paradijs, J., and van der Woerd, H. 1982, *Astr. Ap.*, **113**, 27.  
 Walborn, N. R. 1973, *A.J.*, **78**, 1067.  
 White, N. E., Kallman, T. R., and Swank, J. 1983, *Ap. J.*, **269**, 264.

G. HAMMERSCHLAG-HENSBERGE: Astronomical Institute, University of Amsterdam, Roetersstraat 15, 1018 WB Amsterdam, Netherlands

IAN D. HOWARTH: Department of Physics and Astronomy, University College London, Gower Street, London WC1E 6BT, England  
 [Bitnet: IDH@STAR.UCL.AC.UK]

TIMOTHY R. KALLMAN: Laboratory for High Energy Astrophysics, NASA/Goddard Space Flight Center, Code 665, Greenbelt, MD 20771